

# Transfer Between Invariant Manifolds: From Impulse Transfer to Low-Thrust Transfer

Maxime Chupin, Thomas Haberkorn, Emmanuel Trélat

► **To cite this version:**

Maxime Chupin, Thomas Haberkorn, Emmanuel Trélat. Transfer Between Invariant Manifolds: From Impulse Transfer to Low-Thrust Transfer. *Journal of Guidance, Control, and Dynamics*, American Institute of Aeronautics and Astronautics, 2018, 41 (3), pp.658–672. 10.2514/1.G002922 . hal-01494042v2

**HAL Id: hal-01494042**

**<https://hal.inria.fr/hal-01494042v2>**

Submitted on 8 Dec 2017

**HAL** is a multi-disciplinary open access archive for the deposit and dissemination of scientific research documents, whether they are published or not. The documents may come from teaching and research institutions in France or abroad, or from public or private research centers.

L'archive ouverte pluridisciplinaire **HAL**, est destinée au dépôt et à la diffusion de documents scientifiques de niveau recherche, publiés ou non, émanant des établissements d'enseignement et de recherche français ou étrangers, des laboratoires publics ou privés.

Copyright

# From Impulse Transfer to Low-Thrust Transfer between Invariant Manifolds

Maxime Chupin\*,  
CEREMADE, Université Paris-Dauphine – PSL,  
Thomas Haberkorn†,  
FDP-MAPMO, Université d'Orléans,  
and  
Emmanuel Trélat‡,  
LJLL, Université Pierre et Marie Curie, Paris.

DOI:

**In this work, a new robust and fast method is developed to perform transfers that minimize fuel consumption between two invariant manifolds of periodic orbits in the Circular Restricted Three Body Problem. The method starts with an impulse transfer between two invariant manifolds to build an optimal control problem. This allows to choose an adequate fixed transfer time. Using the Pontryagin Maximum Principle, the resolution of the problem is formulated as that of finding the zero of a shooting function (indirect method). The algorithm couples different kinds of continuations (on cost, final state, and thrust) to improve robustness and to initialize the solver. The efficiency of the method is illustrated with numerical examples. Finally, the influence of the transfer time is studied numerically thanks to a continuation on this parameter, and it checks that when transfer duration goes to zero, the control converges to the impulse transfer that it started with. It shows the robustness of the method, and establishes a mathematical link between the two problems.**

## I. Introduction

Since the late '70s, study of the Circular Restricted Three Body Problem (CRTBP) with the Libration Point Orbits has been of great interest. Indeed, several missions such as ISEE-3 (NASA) in 1978, SOHO (ESA-NASA) in 1996, GENESIS (NASA) in 2001, PLANK (ESA) in 2007 etc. have put this design knowledge into practice. A more profound understanding of the available mission options has also emerged due to the theoretical, analytical, and numerical advances in many aspects of libration point mission design.

There exists a huge number of references on the problem of determining low-cost trajectories by using the properties of the CRTBP and the properties of the equilibrium points called Lagrange or libration points (see [1] and references therein).

Concerning works that use the CRTBP model, in [2, 3], indirect method combined with continuation methods have been used to design missions from an Earth Geostationary Orbit to a Lunar Orbit. The minimum time problem is studied and solved, and continuations between energy and fuel consumption minimizations are performed.

Moreover, in [4], the developed methods involve the minimum-time problem, the minimum energy problem and the minimum fuel problem to reach a fixed point on a Halo orbit starting from a periodic orbit around Earth. Continuations on the thrust are used (indirect methods).

In [5, 6], the author recently developed an efficient method to compute an optimal low-thrust transfer trajectory in *finite* time without using invariant manifolds of the CRTBP. It is based on a three-step solution method using indirect methods and continuations methods and it gives good results.

In these last three contributions, manifolds are not used to help solving the formulated problem but invariant manifolds of the periodic orbits around libration points are a key concept to design interplanetary missions. For a complete point of view on the subject, see [7–10].

These invariant manifolds are separatrices of the dynamics, and so, they can be interpreted as *gravitationally determined pathways* in the three body problem. In [11], and its extension in [12], the network of heteroclinic orbits is obtained. This gives us very interesting tools based on dynamical system methods to design free trajectories with prescribed itineraries.

For instance, in [12–14] are developed very efficient methods to find “zero cost” trajectories between libration point orbits. They used

dynamical system methods to construct heteroclinic orbits from invariant manifolds between Libration Point Orbits. These orbits have been used with impulse engines of spacecrafts to construct finite time transfers.

Following what was done for the patched conic approximation, several restricted three body problems [15] can be connected (patched) and, thanks to invariant manifolds, it is possible to design a map of connections between various areas in the solar system. Indeed, intersections in the position variables between invariant manifolds can be computed and with an impulse,  $\Delta V$ , it is possible to pass from one to another. This principle is the main tool to design the *Interplanetary Transport Network (ITN)* [16] which is a collection of gravitationally determined pathways through the Solar System that require very little energy for an object to follow.

However, the impulse needed to go from one invariant manifold to another cannot be achieved with a low-thrust engine. This is a question in its own, and the purpose of this work is to present a generic new method to address it.

Manifolds have been used in low-thrust mission in [17, 18]. The low-thrust propulsion is introduced by means of special attainable sets that are used in conjunction with invariant manifolds to define a first-guess solution. Then, this solution is improved using an optimal control formalism. One can note that [19] is the first work that combines invariant manifolds and low-thrust in the Earth-Moon system.

In [19, 20], the authors develop direct optimization methods to address such issues. We refer the reader to the textbook [21] for direct methods in aerospace, and to [22] for a short description of the pros and cons of direct versus indirect approaches. In the present work, our objective is to develop an indirect (shooting) method combined with adequate continuations. Numerical homotopies are indeed a good way to overcome the main problem of the shooting method that is the difficulty to initialize it successfully (given that the domain of convergence of the underlying Newton method may be very small). In turn, the fastness and the good numerical accuracy of the shooting method are fully taken advantage of. This is important in view of patching together various three-body problems.

A lot of efforts have been done to design efficient methods to reach periodic orbits, Halo orbits, around equilibrium points in the three body problem. For example, in [23–25], authors use indirect methods and direct multiple shooting methods to reach a manifold's insertion point that goes asymptotically to a Halo orbit in the {Earth-Moon} system. Moreover, using transversality conditions, they optimize the insertion points on the manifold.

\*chupin@ceremade.dauphine.fr

†thomas.haberkorn@univ-orleans.fr

‡emmanuel.trelat@upmc.fr

The outline for the article is as follows. In Sections II, the CRTBP and its properties such as LPOs and invariant manifolds are introduced. In Section III, the method to design trajectories with prescribed itineraries using invariant manifolds and impulse engines is recalled. In section IV, the low-thrust model is introduced. This model does not allow for instantaneous changes in velocity. After that, we explain how an impulse transfer can be used to build an optimal control problem (Section V). To do that both cost functions considered in this work are defined: the  $L^1$ -norm of the control, which corresponds to the physical mass that has to be maximized but which is numerically difficult to optimize, and the  $L^2$ -norm of the control, which corresponds to the physical energy and is smoother. In this part, the continuation performed between these two related problems is introduced.

The last sections are about the general method and the numerical resolution of the previously formulated problems. Indirect methods based on the application of the Pontryagin Maximum Principle (PMP) [26–28] are used, and because the main difficulty of these methods is to initialize them, other continuations for the final state and the thrust to improve robustness are introduced (Section VI). Note that the construction of the optimal control problem starting with the impulse transfer allows to choose an adequate fixed transfer time. The general algorithm is summarized in section VII. In section VIII, different numerical results for different CRTBP are presented. The conclusion is that the method is efficient and can be applied to various systems such as {Earth-Moon} or {Sun-Earth} systems.

In this method, the transfer time is a parameter that is fixed. Of course, the larger the transfer time, the lower the cost ( $L^1$ -norm or  $L^2$ -norm). Moreover, it seems intuitive that the larger the time, the lower the maximum of the control norm during the transfer. A numerical study of the influence of this parameter is performed. Indeed, continuations on the *fixed* transfer time are computed from a (rather) large value to a near zero. It is shown that the control converges to the equivalent impulse transfer  $\Delta V$  as the maximal thrust  $T_{\max}$  goes to infinity. To the best of our knowledge, it is the first time that such a result is obtained. This is a numerical test to check if the method is robust (going to the limit of a small transfer time), and moreover to check if the two problems, impulse and low-thrust one, are somehow connected.

For references on techniques used in our work such as continuation on cost, smoothing techniques and optimization techniques one can read [29–31] as well as [22] where the well-posedness of the continuations is proved.

Initialization of indirect methods with dynamical properties is a real challenge in order to improve the efficiency of indirect methods (see [22] and references therein). Indeed the main difficulties of such methods is to initialize the Newton-like algorithm, and the understanding of the dynamics can be very useful to construct an admissible trajectory for the initialization. Moreover, continuation methods as used in [32] or [33] are crucial to give robustness to these indirect methods.

The algorithm and the method presented in this work constitute a brick for designing interplanetary missions using invariant manifolds in order to take advantage of the Interplanetary Transport Network. A partial application of this algorithm is used in [34] to design a complete mission. This method could be a good first step to initialize missions patching three body problems with some uncontrolled parts (trajectories in invariant manifolds) and some controlled parts computed by this method to connect the invariant manifolds.

## II. The Circular Restricted Three Body Problem

The Circular Restricted Three Body Problem paradigm is used. In this section, the presentation follows the description by [1].

**Problem Description.** We consider the motion of the spacecraft  $P$  of negligible mass moving under the gravitational influence of the two masses  $M_1$  and  $M_2$ , referred to as the primary masses, or simply the *primaries* (here Earth and Moon). These primaries are denoted by  $P_1$  and  $P_2$ . It is assumed that the primaries have circular orbits around their common center of mass. The particle  $P$  is free to move all around the primaries but cannot affect their motion.

In a rotating frame in which the two primaries are fixed and with normalized coordinates (see [1] for details), the coordinates of  $P_1$  and  $P_2$  are respectively  $\xi_{P_1} = (-\mu, 0, 0, 0, 0, 0)$ , and  $\xi_{P_2} = (1-\mu, 0, 0, 0, 0, 0)$ ,

where  $\mu = \frac{M_2}{M_1 + M_2}$  is the *mass parameter*. Let us call  $x_1^0 = -\mu$  and  $x_2^0 = 1 - \mu$ , and by writing the state  $\xi = (x, y, z, \dot{x}, \dot{y}, \dot{z})^T = (x_1, x_2, x_3, x_4, x_5, x_6)^T$ , we obtain

$$\begin{cases} \dot{x}_1 = x_4 \\ \dot{x}_2 = x_5 \\ \dot{x}_3 = x_6 \\ \dot{x}_4 = x_1 + 2x_5 - (1-\mu)\frac{x_1 - x_1^0}{r_1^3} - \mu\frac{x_1 - x_2^0}{r_2^3} \\ \dot{x}_5 = x_2 - 2x_4 - (1-\mu)\frac{x_2}{r_1^3} - \mu\frac{x_2}{r_2^3} \\ \dot{x}_6 = -(1-\mu)\frac{x_3}{r_1^3} - \mu\frac{x_3}{r_2^3} \end{cases} \quad (1)$$

where

$$r_1 = \sqrt{(x_1 - x_1^0)^2 + x_2^2 + x_3^2} \quad \text{et} \quad r_2 = \sqrt{(x_1 - x_2^0)^2 + x_2^2 + x_3^2}$$

are respectively the distances between  $P$  and primaries  $P_1$  and  $P_2$ .

The potential is defined by

$$U(x_1, x_2, x_3) = -\frac{1}{2}(x_1^2 + x_2^2) - \frac{1-\mu}{r_1} - \frac{\mu}{r_2} - \frac{1}{2}\mu(1-\mu). \quad (2)$$

The vector field of the system is denoted by  $F_0$  and the energy of a state point is defined as:

$$\mathcal{E}(\xi) = \frac{1}{2}(\dot{x}^2 + \dot{y}^2 + \dot{z}^2) + U(x, y, z). \quad (3)$$

### A. Libration Point Orbits and Invariant Manifolds

In this Section, some properties of the CRTBP are recalled. In particular, equilibrium points, Libration Points Orbits and invariant manifolds are introduced, for instance see [1, 34–38].

The study of the CRTBP dynamical system shows that around the different equilibrium points of the vector field, there exists periodic orbits (and quasi-periodic orbits) called Libration Point Orbits. A lot of efforts has been dedicated for the theoretical and numerical study of such periodic orbits. Here some properties are recalled.

**Equilibrium Points.** The Lagrange points are the equilibrium points of the circular restricted three-body problem. Euler [39] and Lagrange [40] proved the existence of five equilibrium points: three collinear points on the axis joining the center of the two primaries, generally denoted by  $L_1$ ,  $L_2$  and  $L_3$ , and two equilateral points denoted by  $L_4$  and  $L_5$  (see figure 1).

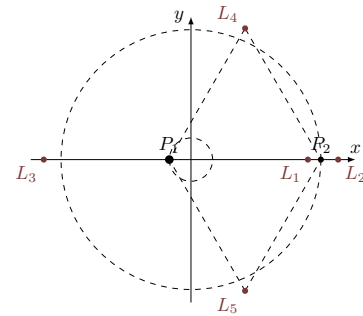


Figure 1: Lagrange points.

Computing equilateral points  $L_4$  and  $L_5$  is not complicated, but it is not possible to find exact solutions for collinear equilibria  $L_1$ ,  $L_2$  and  $L_3$ . A lot of efforts has been dedicated to find series expansion for these points. The solutions from [41] are used. The collinear points are shown to be unstable (in every system), whereas  $L_4$  and  $L_5$  are proved to be stable under some conditions (see [42]).

**Numerical computation of libration point orbits.** The method described in [34] is used to compute the libration point orbits around collinear Lagrange points. This method is based on a shooting method initialized with analytical approximations that can be found in [35–38].

In order to use these orbits to construct various missions, it is very useful to be able to compute the family of periodic orbits given by the well known Lyapunov-Poincaré theorem (see [42, 43]), providing us with different orbits that have different energies. To do that, following [34] a continuation method on the energy parameter is used. Some examples of such periodic orbits are plotted in Figures 2 and 3.

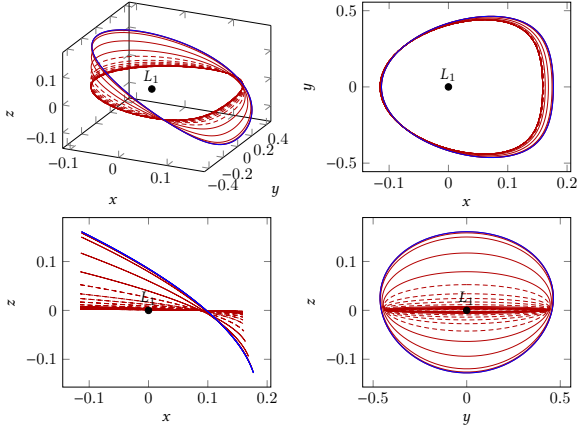


Figure 2: Family of Halo orbits in the {Sun-Earth} system in Richardson coordinates obtained by a Newton-like method and continuation on the energy. The first fixed excursion is  $A_z = 240 \times 10^3$  km and the final energy is  $-1.50042$  in normalized units (corresponding to a quasi-null  $z$ -excursion).

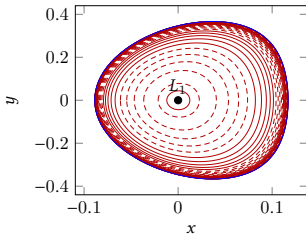


Figure 3: Family of planar Lyapunov orbits in the {Earth-Moon} system in Richardson coordinates obtained by a Newton-like method and continuation on the energy. The final energy is  $-1.6001$  in normalized units.

**Invariant Manifolds.** All periodic orbits described in the previous section generate invariant manifolds, that is to say, the sets of phase points from which the trajectory converges to the periodic orbit, forward for the *stable* manifold and backward for the *unstable* manifold. These manifolds can be very useful to design interplanetary missions because as separatrices, they are gravitationally determined pathways. We refer to [1, chap. 4] for the proof of existence and a more detailed explanation of these manifolds and to [7–10]. The numerical method to compute the invariant manifolds is well known and can be found in the various references of this section such as [1, 7–10, 44]. In Figure 4, the four invariant manifolds for two Lyapunov orbits around  $L_1$  and  $L_2$  in the {Earth-Moon} system are plotted.

### III. Trajectories with Prescribed Itineraries

Invariant manifolds can be used to find trajectories with prescribed itineraries. To illustrate the method, the planar motion of a spacecraft in the {Earth-Moon} system is considered. The realm around Earth is labeled with  $\mathcal{R}_E$ , the realm around the Moon with  $\mathcal{R}_M$  and the exterior realm with  $\mathcal{R}_X$  (see Figure 4). The different realms are defined with the Hill's region which a useful tool to design mission (see Hill's region in [1, 44]). Let us describe a method to find a trajectory with a prescribed itinerary.

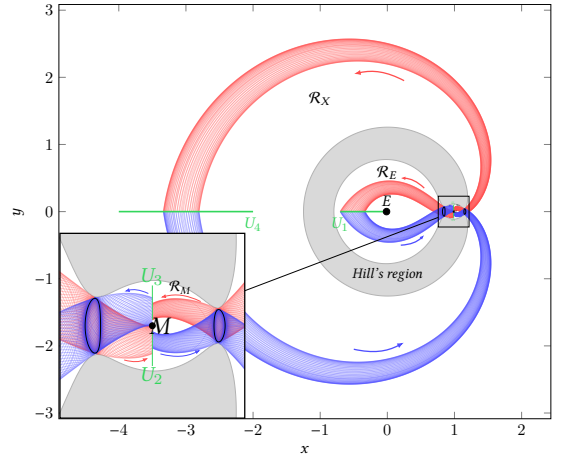


Figure 4: The eight invariant manifolds associated with the Lyapunov orbits of the points  $L_1$  and  $L_2$  in the {Earth-Moon} system, at a specific energy of  $\mathcal{E} = -1.59$ . The different Poincaré surfaces of section  $U_i$  are represented with the Hill's region.

**Step 1.** First, an appropriate energy is chosen. It should allow for motion in the area that has to be reached. Assume that the particle is planned to go between all three realms  $\mathcal{R}_X$ ,  $\mathcal{R}_M$  and  $\mathcal{R}_E$ , then the energy has to be greater than the one of the point  $L_2$ : for instance,  $\mathcal{E} = -1.59$ .

**Step 2.** Two periodic orbits around the two equilibrium points  $L_1$  and  $L_2$  with energy  $\mathcal{E}$  are computed. In Figure 4, we have computed two such Lyapunov orbits.

**Step 3.** The four Poincaré surfaces of section (or Poincaré cuts)  $U_i$ ,  $i \in \{1, \dots, 4\}$  are defined. The surfaces are

$$U_1 = \{(x, y, z); x < 0, y = 0\}, \quad U_2 = \{(x, y, z); x = 1 - \mu, y < 0\}, \\ U_3 = \{(x, y, z); x = 1 - \mu, y > 0\}, \quad U_4 = \{(x, y, z); x < -1, y = 0\}.$$

This way, the  $U_i$  are strategically placed (see [1]): if each  $U_i$  contains the (non empty) intersection between two of the invariant manifolds, then by computing it, a trajectory which connects different realms is found. This result is based on the fact that invariant manifolds are separatrices of the dynamics.

**Step 4.** The invariant manifolds associated with the two periodic orbits are computed as explained previously. They are propagated to the different Poincaré surfaces of section  $U_i$ ,  $i \in \{1, \dots, 4\}$  to obtain the intersection of each manifold with the Poincaré cuts. Figure 4 presents the example of the {Earth-Moon} system. There are eight invariant manifolds, four for each of the two periodic orbits. Thanks to this method it is possible, either to find a trajectory without any impulse respecting the prescribed itinerary, or, one with a finite number of impulses (for instance, when an intersection is found in the positions of two invariant manifolds but with a velocity gap).

## IV. Modeling

### A. Controlled Dynamics

The model for the evolution of our spacecraft in the CRTBP is described. In non normalized coordinates, the controlled dynamical system is

$$m(t) \frac{d\mathbf{R}(t)}{dt} = -GM_1 m(t) \frac{\mathbf{R}_{13}(t)}{R_{13}^3(t)} - GM_2 m(t) \frac{\mathbf{R}_{23}(t)}{R_{23}^3(t)} + T(t),$$

where  $T$  is the spacecraft driving force, and  $m$  is the time-dependent mass of the spacecraft. The equation of evolution of the mass is  $\dot{m}(t) = -\beta \|T(t)\|$ , where  $\beta$  is computed from two parameters  $I_{sp}$  and  $g_0$ :  $\beta$  is equal to  $\frac{1}{I_{sp} g_0}$  and its units is second per meter. In this work, the values for these parameters are  $I_{sp} = 2000$  s, and  $g_0 = 9.81$  m/s<sup>2</sup>.

Moreover, the thrust is constrained as follows, for all  $t$ ,  $\|T(t)\| \leq T_{\max}$ , where  $T_{\max} > 0$  is the maximal thrust that the engine can generate.

Using the normalization parameters, the normalized counterpart of  $\beta$  is denoted by  $\beta_*$  and the coefficient  $\frac{t_2^2}{4\pi^2 t_*} T_{\max}$  by  $\epsilon$ . Furthermore, the thrust becomes  $T(t) = \epsilon u(t)$  where for all  $t$ ,  $\|u(t)\| \leq 1$  in the normalized system. In condensed form, the system is written as :

$$\begin{cases} \dot{x} = F_0(x) + \frac{\epsilon}{m} \sum_{i=1}^3 u_i F_i(x), \\ \dot{m} = -\beta_* \epsilon \|u\|, \end{cases}$$

where  $F_0$  is defined in (1) and

$$F_1(x) = \begin{pmatrix} 0 \\ 0 \\ 0 \\ 1 \\ 0 \\ 0 \end{pmatrix}, F_2(x) = \begin{pmatrix} 0 \\ 0 \\ 0 \\ 0 \\ 1 \\ 0 \end{pmatrix}, F_3(x) = \begin{pmatrix} 0 \\ 0 \\ 0 \\ 0 \\ 0 \\ 1 \end{pmatrix}.$$

**Remark:** This system belongs to a well known class of controlled systems: the affine control systems.  $F_0$  is called a *drift vector field* while the  $F_i$  are called *control vector fields*. Let us note that for these systems, geometric control theory is helpful to establish controllability properties (see [45, 46]).

**Controllability.** In [2], it is proved that the CRTBP with a non evolving mass is controllable for a suitable subregion of the phase-space, where the energy is greater than the energy of  $L_1$ . Thanks to [47, Prop. 2.2], one can extend this result to the system with an evolving mass.

## V. Construction of an Optimal Control Problem (OCP)

In the previous sections, we have recalled how a mission can be designed using *impulse* and *invariant manifolds* to save a lot of propellant. Invariant manifolds are separatrices of the dynamics and act as the *gravitationally determined pathways*.

The model for the low-thrust engine spacecraft has been introduced. Because of the low-thrust engine, the method presented in section III for mission design cannot be applied. Indeed, to go from one invariant manifold to another, an instantaneous change of velocity is not possible anymore.

For this reason, we develop a method to connect two invariant manifolds using low-thrust. With this model, the natural context is optimal control theory. Indeed, because the control is permanent during the transfer time, one can write the minimization of the mass consumption in terms of an integral of the control norm.

First, let us introduce an optimal control problem to perform the transfer between two invariant manifolds.

### A. From an Impulse Solution to an Optimal Control Problem

First, an impulse transfer between two manifolds is considered. The two considered invariant manifolds are denoted respectively by  $\mathcal{M}_0$  and  $\mathcal{M}_1$ . The goal of this section is to find a trajectory performing the transfer between these two invariant manifolds.

**Remark:** The choice of the two invariant manifolds  $\mathcal{M}_0$  and  $\mathcal{M}_1$  depends on the complete mission that has to be designed. Indeed, keep in mind that a transfer between two invariant manifolds can be viewed as the cornerstone of a complete mission design.

Of course, the two invariant manifolds should be chosen such that the transfer from one to another is useful. For example, they must be “oriented” in the same direction. Moreover, the two chosen invariant manifolds must be such that there exists a section where the distance in position and velocity is not too large.

These notions are not mathematically well defined here, but the key is the knowledge of the map of invariant manifolds.

## B. The Impulse Transfer

Considering an impulse transfer between  $\mathcal{M}_0$  and  $\mathcal{M}_1$ , a Poincaré surface of section is defined and denoted by  $U$  where there exists an intersection in position of the two invariant manifolds. Denote by  $\xi_0^U = (\mathbf{x}_0^U, \mathbf{v}_0^U)$  and  $\xi_1^U = (\mathbf{x}_1^U, \mathbf{v}_1^U)$  the two points in this surface of section where  $\mathbf{x}_i^U = (x_1^i, x_2^i, x_3^i) = (x_i, y_i, z_i)$ ,  $i \in \{0, 1\}$ , and  $\mathbf{v}_i^U = (x_4^i, x_5^i, x_6^i) = (\dot{x}_i, \dot{y}_i, \dot{z}_i)$ ,  $i \in \{0, 1\}$ , and such that  $\mathbf{x}_0^U = \mathbf{x}_1^U$ . Denote by  $\mathcal{A}_0$  (resp.  $\mathcal{A}_1$ ) the orbit to which  $\xi_0^U$  (resp.  $\xi_1^U$ ) belongs. Hence, to go from  $\mathcal{A}_0$  belonging to  $\mathcal{M}_0$  to  $\mathcal{A}_1$  belonging to  $\mathcal{M}_1$ , the impulse  $\Delta V = \mathbf{v}_1^U - \mathbf{v}_0^U$  has to be performed.

Thanks to that, the spacecraft is able to go from one orbit belonging to the first manifold to another belonging to the second manifold (see Figure 5).

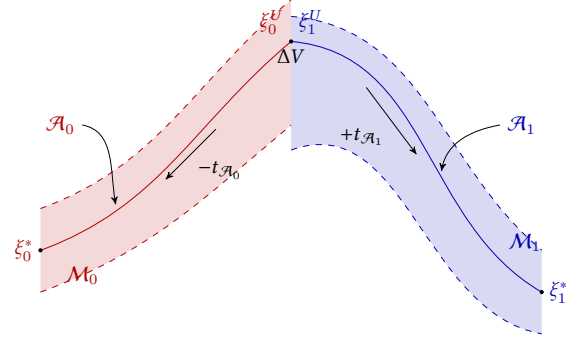


Figure 5: Drawing of the construction of the terminal points of the optimal control problem starting with an impulse transfer between invariant manifolds  $\mathcal{M}_0$  and  $\mathcal{M}_1$ .

**Intersection Problem.** Different cases are in order:

1. If the *planar case* is considered, then there are four state variables ( $\xi \in \mathbb{R}^4$ ) on the surface of section  $U$ , we look for an intersection in  $\mathbb{R}^3$ . Moreover, if both manifolds share the same energy, then a complete intersection in position and velocity is possible (not guaranteed). In that case, the transfer can be performed without any control. See the section on heteroclinic and homoclinic orbits in [1, 44].
2. If the *planar case* is considered but without the same energy for the two invariant manifolds, then it is possible to find a position intersection, but with a gap in velocity. Once again, the existence is only empirical.
3. If the *spatial case* is considered, then the state  $\xi \in \mathbb{R}^6$  so on the surface of section  $U$ , we look for an intersection in  $\mathbb{R}^5$ . In that case, an intersection is difficult to find and, we actually give up searching for such a point. Instead, an intersection is computed in the position space only. This can be done by a bisection method using the projection on the Poincaré surface.

Note that this method can be applied when there is no intersection (nor in position nor in velocity), but with a small  $\Delta\xi = (\Delta\mathbf{x}, \Delta\mathbf{v}) = (\mathbf{x}_1^U - \mathbf{x}_0^U, \mathbf{v}_1^U - \mathbf{v}_0^U)$ , where  $\mathbf{x} = (x_1, x_2, x_3) = (x, y, z)$  and  $\mathbf{v} = (x_4, x_5, x_6) = (\dot{x}, \dot{y}, \dot{z})$  depending of the notation. For pedagogical reason, the case with only a  $\Delta V$  is considered.

## C. Optimal Control Problem

Thanks to the impulse transfer between the two invariant manifolds, two trajectories  $\mathcal{A}_0 \in \mathcal{M}_0$  and  $\mathcal{A}_1 \in \mathcal{M}_1$  are computed and two points  $\xi_0^U \in \mathcal{A}_0$  and  $\xi_1^U \in \mathcal{A}_1$  such that  $\xi_1^U - \xi_0^U = (0, \Delta V)$ .

**Perturbation Times.** Starting with these two points  $\xi_0^U \in \mathbb{R}^6$  and  $\xi_1^U \in \mathbb{R}^6$ , two times  $t_{\mathcal{A}_0}$  and  $t_{\mathcal{A}_1}$  are chosen to respectively propagate backward the point  $\xi_0^U$  and forward the  $\xi_1^U$ . Mathematically, denoting by  $\phi^{\text{nat}}$  the flow of the (uncontrolled) natural dynamics, two points in  $\mathbb{R}^6$  are defined by  $\xi_0^* = \phi^{\text{nat}}(-t_{\mathcal{A}_0}, \xi_0^U)$ , and  $\xi_1^* = \phi^{\text{nat}}(t_{\mathcal{A}_1}, \xi_1^U)$ . See Figure 5 for an illustration of this construction.

**Optimal Control Problem Formulation.** Let us define a new transfer time  $t_f$  such that  $t_f = t_{\mathcal{A}_0} + t_{\mathcal{A}_1}$ .

It is now possible to define the optimal control problem. The criterion that has to be maximized is the final mass (this in turn minimizes the amount of propellant burnt during the mission). Indeed, because the real cost for the launch of the spacecraft is to send it “away from Earth”, *i.e.*, to send it to a first *parking orbit* around Earth (for example a *low Earth orbit* is the simplest and cheapest for spacecraft positioning), the lighter the spacecraft, the cheaper the launch.

The problem of the maximization of the final mass is equivalent to the minimization of the  $L^1$ -norm of the control  $u$ . Therefore the problem that has to be solved is the following:

$$\mathcal{P}_{L^1} \begin{cases} C_{L^1}(u) = \int_0^{t_f} \|u\| dt \rightarrow \min, \\ \dot{x} = F_0(x) + \frac{\epsilon}{m} \sum_{i=1}^3 u_i F_i(x), \\ \dot{m} = -\beta_* \epsilon \|u\|, \\ \|u\| \leq 1, \\ x(0) = \xi_0^*, m(0) = m_0^*, \text{ and } x(t_f) = \xi_1^*. \end{cases} \quad (4)$$

**Remark:** Because we want to maximize the final mass, the transfer time must be fixed. Indeed, the larger the transfer time, the higher the final mass.

The choice of the transfer time is a difficult problem and thanks to the construction of the terminal points  $\xi_0^*$  and  $\xi_1^*$  (following the uncontrolled dynamics), a transfer time is chosen which is adequate, in order to ensure that the problem that we address is indeed feasible.

## D. Control Structure

### 1. Minimization of the $L^1$ -norm of the Control

In this section, the Pontryagin Maximum Principle (PMP) is applied to the problem (4) to get the structure of the control (see [26–28]). The costate denoted by  $(p^0, p, p_m) = (p^0, p_x, p_v, p_m)$  is introduced and associated with the state denoted by  $(\xi, m) = (x, v, m)$ . The Hamiltonian of the system is

$$\begin{aligned} \mathcal{H}(x, m, u, p^0, p, p_m) &= (p^0 - \beta_* \epsilon p_m) \|u\| + H_0 + u_1 \frac{\epsilon}{m} H_1 \\ &\quad + u_2 \frac{\epsilon}{m} H_2 + u_3 \frac{\epsilon}{m} H_3, \end{aligned}$$

where  $H_i = \langle p, F_i \rangle$  for  $i \in \{0, \dots, 3\}$ . The application of the PMP yields

$$\begin{aligned} \dot{x} &= \frac{\partial \mathcal{H}}{\partial p}(x, u, p), \quad \dot{p} = -\frac{\partial \mathcal{H}}{\partial x}(x, u, p), \\ u(t) &= \arg \max_{\|v\| \leq 1} \mathcal{H}(x, m, v, p^0, p, p_m). \end{aligned}$$

In order to obtain the structure of the optimal control, results from the contributions in [32, Prop. 2.3.] extended to the CRTBP in [3] are recalled.

Thanks to these results, the normal case (see [48]) is considered, that is to say that  $p^0 \neq 0$ , so the costate  $(p^0, p)$  can be normalized with  $p^0 = -1$ .

Defining  $\varphi(p) = (H_1, H_2, H_3)$  and denoting by  $\zeta = (x, m, p, p_m)$ , let us introduce the *switching function*  $\psi(\zeta) = 1 - \beta_* \epsilon p_m - \frac{\epsilon}{m} \|\varphi(p)\|$ . Then, the optimal control is:

- if  $\|\varphi(p)\| \neq 0$ , then

$$\begin{cases} u(\zeta) = 0 & \text{if } \psi(\zeta) < 0, \\ u(\zeta) = \alpha \frac{\varphi(p)}{\|\varphi(p)\|}, \quad \alpha \in [0, 1] & \text{if } \psi(\zeta) = 0, \\ u(\zeta) = \frac{\varphi(p)}{\|\varphi(p)\|} & \text{otherwise,} \end{cases}$$

- if  $\|\varphi(p)\| = 0$ , then

$$\begin{cases} u(\zeta) = 0 & \text{if } \psi(\zeta) < 0, \\ u(\zeta) \in \mathbf{B}(0, 1) & \text{if } \psi(\zeta) = 0, \\ u(\zeta) \in \mathbf{S}(0, 1) & \text{otherwise,} \end{cases}$$

where  $\mathbf{S}(a, b)$  is the  $\mathbb{R}^3$ -sphere centered on  $a$  with radius  $b$ , and  $\mathbf{B}(a, b)$  is the  $\mathbb{R}^3$  ball.

**Remark:** [Singular Arcs] Note that the case  $\|\varphi(p)\| = 0$  can be a problem. However, one can prove that  $\|\varphi(p)\|$  has a finite number of zeros along a solution and the assumption that it remains true on a neighborhood of the solution guarantees that the numerical evaluation of the control is not problematic as long as there are no singular arcs. Hence,  $\varphi$  is assumed to have a finite number of zeros.

This assumption can be checked *a posteriori*, once the numerical computation has been performed.

**Shooting Function.** The structure of the control has been established using the maximization condition of the PMP. Then, the resolution of the problem is equivalent to finding the root of a shooting function.

First, the free final mass transversality condition gives  $p_m(t_f) = 0$ . Because fixed end points  $\xi_0^*$  and  $\xi_1^*$  are considered, transversality conditions for the costate  $p$  associated to the state  $x$  do not give any information. The boundary value problem defined by the application of the PMP is reduced to find initial costate values  $(p(0), p_m(0))$  such that the extremal solution  $\zeta(\cdot) = (x(\cdot), m(\cdot), p(\cdot), p_m(\cdot))$  is well defined and reach the final state  $x(t_f) = \xi_1^*$  starting at  $(x(0), m(0)) = (\xi_0^*, m_0^*)$ . Finally, the shooting function can be written as

$$\mathcal{S}_{L^1}(p(0), p_m(0)) = \begin{pmatrix} \phi_{1,\dots,6}^{\text{ext}}(\xi_0^*, m_0^*, p(0), p_m(0)) - \xi_1^* \\ \phi_{14}^{\text{ext}}(\xi_0^*, m_0^*, p(0), p_m(0)) \end{pmatrix} = \begin{pmatrix} 0 \\ 0 \end{pmatrix}$$

where  $\phi^{\text{ext}}$  is the flow of the extremal dynamics given by the PMP.

To solve such a problem, a Newton-like method is used. For that kind of method, the shooting function has to be differentiable. As noticed in [22, 29, 32], the shooting function remains differentiable in a neighborhood of an optimal trajectory under generic conditions (for instance, a neighborhood in which the same bang-bang structure is preserved).

*With the assumption on singular arcs, the minimization of the  $L^1$ -norm of the control leads to a control called bang-bang, indeed  $\|u\|$  alternates between  $\|u\| = 0$  and  $\|u\| = 1$ .*

*Numerically, this problem is difficult to solve. Indeed, one has to know, a priori, the structure of the controlled solution, and the search for zeros of the shooting function is hard to initialize.*

*To overcome this difficulty, a continuation from a simpler problem is used: the  $L^2$ -norm of the control minimization.*

### 2. Minimization of the $L^2$ -norm of the Control

Consider the same problem as the one defined by 4, but with the following criterion to minimize:

$$C_{L^2}(u) = \int_0^{t_f} \|u\|^2 dt \rightarrow \min. \quad (5)$$

The problem is simpler because the optimal control is not *bang-bang* anymore (that will be clearer with the analysis of the structure of the optimal control) and the solution of this problem is used as the initial problem for a continuation to solve problem (4). Problem (5) has a cost defined by the  $L^2$ -norm of the control. This cost corresponds to the minimization of the energy.

For the sake of conciseness, the family of problems denoted by  $\mathcal{P}_{C,\lambda}$ , indexed by  $\lambda \in [0, 1]$ , is introduced considering the same problem defined by 4, but with the following criterion to minimize:

$$C_\lambda(u) = \int_0^{t_f} \left( (1-\lambda) \|u\|^2 + \lambda \|u\| \right) dt \rightarrow \min. \quad (6)$$

Indeed, the analysis of the control structure is the same for problems (5) and (6) for  $\lambda \in [0, 1[$ . The Hamiltonians of these problems are

$$\begin{aligned} \mathcal{H}_\lambda(x, m, u, p^0, p, p_m) &= (-\lambda - \beta_* \epsilon p_m) \|u\| - (1-\lambda) \|u\|^2 + H_0 \\ &\quad + u_1 \frac{\epsilon}{m} H_1 + u_2 \frac{\epsilon}{m} H_2 + u_3 \frac{\epsilon}{m} H_3. \end{aligned} \quad (7)$$

We get the optimal control

- if  $\|\varphi(p)\| \neq 0$ , then

$$\begin{cases} u(\zeta) = 0 & \text{if } \psi_\lambda(\zeta) \leq 0, \\ u(\zeta) = \psi_\lambda(\zeta) \frac{\varphi(p)}{\|\varphi(p)\|} & \text{if } \psi_\lambda(\zeta) \in [0, 1], \\ u(\zeta) = \frac{\varphi(p)}{\|\varphi(p)\|} & \text{otherwise,} \end{cases} \quad (8)$$

- if  $\|\varphi(p)\| = 0$ , then

$$\begin{cases} u(\zeta) = 0 & \text{if } \psi_\lambda(\zeta) \leq 0, \\ u(\zeta) \in \mathbf{S}(0, \psi(\zeta)) & \text{if } \psi_\lambda(\zeta) \in [0, 1], \\ u(\zeta) \in \mathbf{S}(0, 1) & \text{otherwise,} \end{cases}$$

where  $\mathbf{S}(a, b)$  is the  $\mathbb{R}^3$ -sphere centered on  $a$  with radius  $b$ .

The shooting function is exactly the same as before but the control is different, and so are the extremal dynamics. The result on the regularity of the shooting function still holds, because the shooting function for  $\lambda < 1$  is more regular than the one for  $\lambda = 1$  (the control is now continuous).

## VI. Additional Continuations

The main results have now been established for the two problems to solve: the  $L^1$ -norm minimization of the problem  $(\mathcal{P}_{L^1})$ , the  $L^2$ -norm minimization of the problem  $(\mathcal{P}_{L^2})$  as well as all continuations between the two problems with the family of problems  $(\mathcal{P}_{C_\lambda})$ . This continuation is used in various references in different contexts such as two body problem (see [32]) and CRTBP (see [3]).

However, the transfer is still too difficult to initialize. Indeed, we still do not know how to initialize the simpler problem  $\mathcal{P}_{L^2}$ .

To achieve this, several continuations are combined that are of different kinds: one on the final state, another one on the maximal value of the thrust, and another one on the cost functional. The overall method is a good way for automatically initializing the solving. The order in which the continuations are performed is important (some paths do not work). The structure of the algorithm is represented in Figure 7.

In this section two additional continuations are introduced in the complete algorithm.

### A. Final State Continuation

Let us start with the first continuation in our multistep method. The problem described in Section A is considered, that is to say, with the  $L^2$ -norm of the control as the cost function  $(\mathcal{P}_{L^2})$ .

Instead of the final state  $\xi_1^*$ , the point  $\xi_1^{\text{nat}}$  defined by  $\xi_1^{\text{nat}} = \phi^{\text{nat}}(t_f, \xi_0^*)$  is considered. In simple words, the initial point is just propagated following the natural dynamics during the transfer time. See Figure 6 for an illustration. It is obvious then that solving the optimal control problem  $(\mathcal{P}_{L^2})$  with  $\xi_1^* = \xi_1^{\text{nat}}$  is very easy.

Indeed, a *constant null control*, with a null costate, constitutes the optimal extremal solution which follows the natural dynamics.

One can then construct a continuation of problems to solve  $\mathcal{P}_{L^2}$  using the following family of problems depending continuously on the parameter  $\lambda \in [0, 1]$  (see Figure 6 for an illustration)

$$\mathcal{P}_{\text{FS}}^\lambda \begin{cases} C_{L^2}(u) = \int_0^{t_f} \|u\|^2 dt \rightarrow \min, \\ \dot{x} = F_0(x) + \frac{\epsilon}{m} \sum_{i=1}^3 u_i F_i(x), \\ \dot{m} = -\beta_* \epsilon \|u\|, \\ \|u\| \leq 1, \\ x(0) = \xi_0^*, m(0) = m_0^*, \text{ and } x(t_f) = (1 - \lambda)\xi_1^{\text{nat}} + \lambda\xi_1^*. \end{cases}$$

This problem is associated to the corresponding shooting function

$$\mathcal{S}_{\text{FS}}^\lambda(p(0), p_m(0)) = \begin{pmatrix} \phi_{1,\dots,6}^{\text{ext}}(\xi_0^*, m_0^*, p(0), p_m(0)) - \xi_1^\lambda \\ \phi_{14}^{\text{ext}}(\xi_0^*, m_0^*, p(0), p_m(0)) \end{pmatrix} = \begin{pmatrix} 0 \\ 0 \end{pmatrix},$$

where  $\xi_1^\lambda = (1 - \lambda)\xi_1^{\text{nat}} + \lambda\xi_1^*$ .

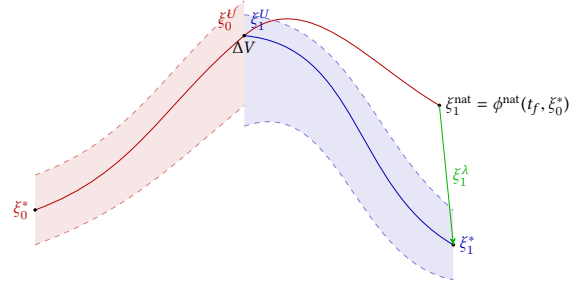


Figure 6: Illustration of the continuation on the final state.  $\xi_1^{\text{nat}}$  is the propagation of the initial point  $\xi_0^*$  during the transfer time  $t_f$ . Step by step, we reach the final point  $\xi_1^\lambda = (1 - \lambda)\xi_1^{\text{nat}} + \lambda\xi_1^*$ , with  $\lambda$  going from 0 to 1.

### B. Thrust Continuation

The low level of the thrust is also an issue. Indeed, the lower the magnitude of the maximal thrust, the smaller the attainable set, and so the more difficult the problem is to initialize. To overcome this difficulty, another continuation is used, but this time, on the maximal thrust.

Let  $\epsilon_{\text{obj}}$  be the maximal thrust corresponding to the real engine and a greater thrust  $\epsilon_{\text{init}}$ . For instance, consider the example of  $\epsilon_{\text{obj}}$  corresponding to 0.3 N and  $\epsilon_{\text{init}}$  corresponding to 60 N. We denote by  $\epsilon_\lambda = (1 - \lambda)\epsilon_{\text{init}} + \lambda\epsilon_{\text{obj}}$ , the intermediary thrust that allows us to define the following family of problems for all  $\lambda \in [0, 1]$ .

$$\mathcal{P}_{\text{thrust}}^\lambda \begin{cases} C_{L^2}(u) = \int_0^{t_f} \|u\|^2 dt \rightarrow \min, \\ \dot{x} = F_0(x) + \frac{\epsilon_\lambda}{m} \sum_{i=1}^3 u_i F_i(x), \\ \dot{m} = -\beta_* \epsilon_\lambda \|u\|, \\ \|u\| \leq 1, \\ x(0) = \xi_0^*, m(0) = m_0^*, \text{ and } x(t_f) = \xi_1^*. \end{cases}$$

## VII. Description of the Algorithm: From Impulse Transfer to Low-Thrust Transfer

An algorithm (implemented in C++) has been developed to solve the problem of performing the transfer between two *natural* trajectories of two invariant manifolds (but not only). In this section, this algorithm is briefly described.

### A. Principle

The main idea is described by the following items and summarized in Figure 7.

- Start with the two points denoted by  $\xi_0^U$  and  $\xi_1^U$  in Section A and Figure 5. These points are chosen in such a way that they minimize the distance between the two intersections between invariant manifolds and the Poincaré cut we chose.
- Choose two times of propagation  $t_{\mathcal{A}_0}$  and  $t_{\mathcal{A}_1}$  to build the end-points of the transfer and an additional parameter  $\alpha_T \in ]0, 1[$ . This parameter allows to start the resolution with two points denoted by  $\xi_0^{\alpha T}$  and  $\xi_1^{\alpha T}$  and defined as  $\xi_0^{\alpha T} = \phi(-\alpha_T t_{\mathcal{A}_0}, \xi_0^U)$  and  $\xi_1^{\alpha T} = \phi(\alpha_T t_{\mathcal{A}_1}, \xi_1^U)$ . The two times of propagation  $t_{\mathcal{A}_0}$  and  $t_{\mathcal{A}_1}$  define a total *fixed* transfer time for the problem:  $t_f = t_{\mathcal{A}_0} + t_{\mathcal{A}_1}$ . These two points are closer than the two end-points defined as  $\xi_0^* = \phi(-t_{\mathcal{A}_0}, \xi_0^U)$  and  $\xi_1^* = \phi(t_{\mathcal{A}_1}, \xi_1^U)$ . The two objective states  $\xi_0^*$  and  $\xi_1^*$  are reached by continuation on the initial and final state as described in Section A.<sup>a</sup>
- A (boolean) parameter is given to activate the continuation between the minimization of the  $L^2$ -norm of the control and the

<sup>a</sup>The continuation on the initial state can easily be derived from the explanation of the final state continuation.

minimization of the  $L^1$ -norm. If it is active, then, to overcome some numerical difficulties, another parameter is added, to indicate the position of this continuation in the algorithm (see Figure 7).

- If two different maximal thrusts are given, the algorithm performs a continuation on the thrust as explained in Section B.
- Checking the  $L^i$ -norm of the control ( $i \in \{1, 2\}$ ) during the thrust continuation, it is checked if the border of the accessible set is reached (or at least get an indication of whether this is the case). If so, then the transfer time is increased by another continuation on this parameter.

Of course, the initialization of a non zero costate is allowed to help convergence of the first step of the algorithm.

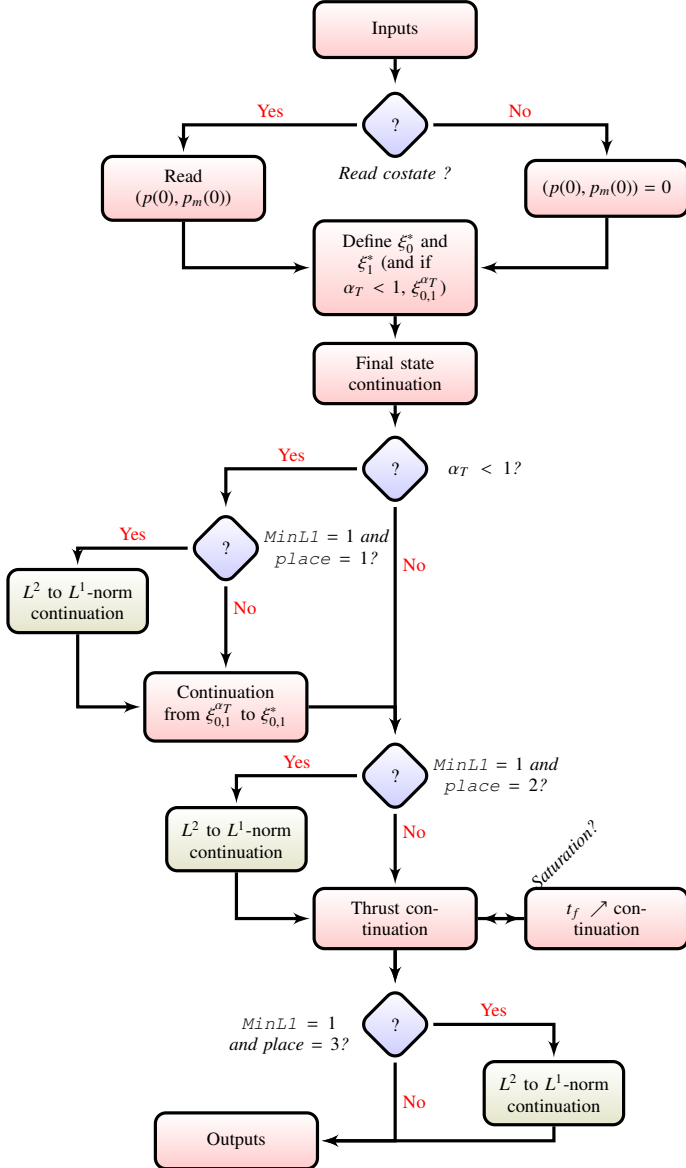


Figure 7: Description of the algorithm to solve the transfer between invariant manifolds with low thrust.

### 1. Numerical Codes

Although there exists excellent software to perform continuations for optimal control problem such as the well-known Hompack90 [49] or Hampath [33], because of the structure of the algorithm of this method, we chose to write our own code.

The code used is C++, with interfaces to some very efficient FORTRAN codes. The program is based on the following librairies:

- the DOP853 explicit step-varying Runge-Kutta method developed by [50]. To verify the implementation of the method, another integrator is available, `ode.f`, by Shampine and Gordon, which can be found on the [netlib.org](http://netlib.org) website.
- For the Newton-like method, we used the well known FORTRAN code: the MINPACK subroutine HYBRD by Burton S. Garbow, Kenneth E. Hillstom, Jorge J. More. One can find a F90 version `hbrd.f`, by A. Miller. These two versions are implementations of Powell's Hybrid algorithm used to solve systems of nonlinear equations.

## VIII. Numerical Results

In this section, the developed method is used to compute real transfers between invariant manifolds.

### A. Transfer between Invariant Manifolds: {Earth-Moon} System, Halo Orbits

Let us consider once again the {Earth-Moon} system, and two Halo orbits around  $L_1$  and  $L_2$  with different energies. In table 1, the initial conditions and the periods for the two considered Halo orbits are given. These two Halo orbits have been computed with the same  $z$ -excursion of  $16 \times 10^3$  km. We refer to [1] for the values of all the constants for various CRTBPs of the solar system.

	$x$	$y$	$z$
Halo $L_1$	8.23362033247E-01	0.0E+00	4.16230924917E-05
Halo $L_2$	1.12040065667E+00	0.0E+00	4.16230924917E-05
	$\dot{x}$	$\dot{y}$	$\dot{z}$
Halo $L_1$	0.0E+00	1.26343508887E-01	0.0E+00
Halo $L_2$	0.0E+00	1.76071039637E-01	0.0E+00
Period			
Halo $L_1$	2.74294400617E+00		
Halo $L_2$	3.41558381117E+00		

Table 1: Initial conditions and periods for the two Halo orbits around  $L_1$  and  $L_2$  used to perform the transfer between their invariant manifolds. Values are expressed in the normalized system of units of the {Earth-Moon} system.

The method that was previously described is followed:

1. Compute the manifolds from the two periodic orbits around  $L_1$  and  $L_2$ . Here, Halo orbits (which are diffeomorphic to a circle) are considered. See Figure 2 for a plot of such an orbit.
2. Compute the intersections with the Poincaré cut  $U_2$ . See Figure 8. The different projections onto the  $(y, z)$ -plane are plotted (recall that  $x$  is set to  $1 - \mu$  on  $U_2$ ), the  $(y, \dot{y})$ -plane and the  $(z, \dot{z})$ -plane.
3. Compute the two points  $\xi_0^U$  and  $\xi_1^U$  that minimize  $\Delta\xi = \|\xi_0^U - \xi_1^U\|$ . Note that here there is not only a  $\Delta v = \Delta v$  but also a  $\Delta x$ .
4. Choose two times, previously denoted by  $t_{\mathcal{A}_0}$  and  $t_{\mathcal{A}_1}$ . Here, we choose 0.5 for both times, expressed in the normalized system of units. This corresponds to a total travel time of 4.34 days. Thanks to this choice, the two end-points can be built, they are denoting by  $\xi_0^*$  and  $\xi_1^*$ . The two natural trajectories are plotted in Figure 9.

The final state continuation ( $\mathcal{P}_{\text{FS}}^1$ ) is straightforward as long as the maximal thrust is large enough. In Figure 10a, the norm of the control is plotted during each step of the final state continuation, and even though the final control is smaller than 0.55 N, it reaches nearly 3 N during the continuation.

Here, the computation of the transfer starts with a maximal thrust of 60 N to reach 0.45 N by the continuation ( $\mathcal{P}_{\text{thrust}}^1$ ). See Figure 10b for



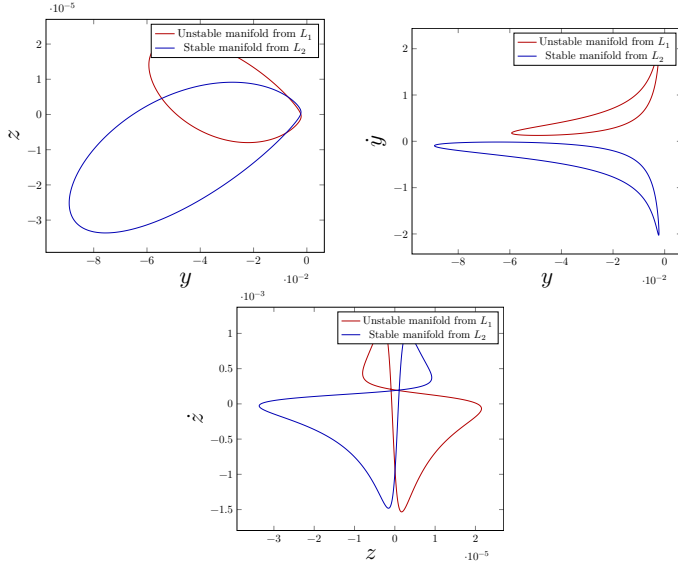


Figure 8: {Earth-Moon} system: Different projections of the intersection with the Poincaré cut  $U_2$  for the invariant manifolds associated with the two Halo orbits around  $L_1$  and  $L_2$ . Note that there is no intersection between the two manifolds, and this is obvious with the  $(y, \dot{y})$ -plane projection.

the plot of the evolution of the control norm with respect to time during the continuation. One can observe that the control is saturated only along the last step of the continuation. Indeed, for a maximal thrust greater than 0.55 N, the control is not saturated, and so, the continuation on the maximal thrust does not change the optimal control, until reaching the critical value. One can think that it is useless to start this continuation with the value of 60 N, but, for instance, if it starts with a value of 1 N, the final state continuation fails. Even though the control is not saturated, a large starting value provides us with a suitable attainable set, and allows the final state continuation to converge. This way the continuation on the thrust is very fast, and smooth.

The continuation on the cost ( $\mathcal{P}_{C_1}$ ) between the  $L^2$ -norm and the  $L^1$ -norm is then performed and succeeds easily. The different steps in the continuation for the norm of the control are plotted in Figure 10c.

The final trajectories are plotted in Figure 9. The trajectories for both the  $L^1$ -minimization and the  $L^2$ -minimization are very close to each other and differences cannot be seen on the plot. Obviously, the longer the transfer time is (that is to say the choice of  $t_{\mathcal{A}_0}$  and  $t_{\mathcal{A}_1}$ ), the smaller both the  $L^1$ -cost and  $L^2$ -cost are.

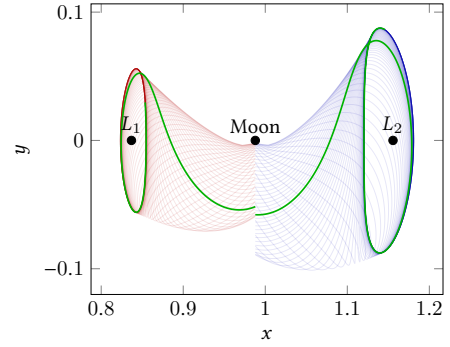
Because only indirect methods are used, the computation of the transfer, including all steps and continuations, only takes 13.18 s on a standard desktop computer. Each of the three continuations is very efficient, and they converge in, respectively, 19, 20 and 22 iterations. The initial mass is 1500 kg for the spacecraft, and the final mass is 1492.885 68 kg for the minimization of the  $L^1$ -norm of the control.

**Remark:** This transfer method can be used to design a complete mission initialized with several controlled and uncontrolled parts, the uncontrolled ones being trajectories belonging to invariant manifolds.

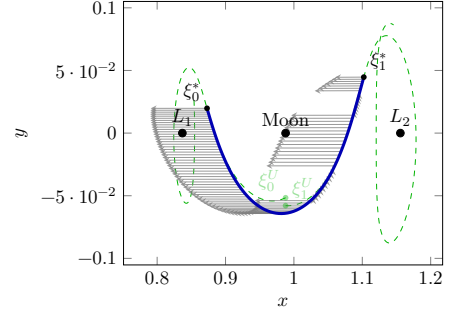
This is the idea of this work: we want to use, as explained in the introduction, the invariant manifolds in the Interplanetary Transport Network [16], connected by small optimal transfers between invariant manifolds, to initialize the complete mission. The final mission will consist of several uncontrolled parts (following the invariant manifolds) and controlled parts (the connection between manifolds computed with our algorithm).

## B. Transfer between Invariant Manifolds: {Sun-Earth} System, Halo Orbits

This time the {Sun-Earth} system is considered, and two Halo orbits around  $L_1$  and  $L_2$  with different energies, respectively  $\mathcal{E}_{L_1} =$



(a) Intersection of the two invariant manifolds, and the two trajectories that correspond to  $\xi_0^U$  and  $\xi_1^U$  that minimize the distance between the two sections.



(b) Optimal solutions for the transfer between the two invariant manifolds. The solutions for the minimization of the  $L^2$ -norm of the control and the solution for the  $L^1$ -norm overlap because of the tiny difference between them.

Figure 9: {Earth-Moon} system: Construction and solving of the transfer problem between the two invariant manifolds of two Halo orbits around  $L_1$  and  $L_2$ .

$-1.500444$  and  $\mathcal{E}_{L_2} = -1.500443$ . In table 2, the initial conditions and the periods for the two considered Halo orbits are given. Once again, we refer to [1] for the values of all the constants for various CRTBPs of the solar system.

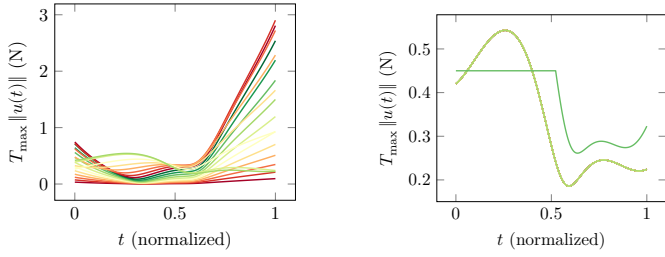
	$x$	$y$	$z$
Halo $L_1$	9.88877586385E-01	0.0E+00	4.01075229212E-06
Halo $L_2$	1.00838140029E+00	0.0E+00	1.61657961732E-05
	$\dot{x}$	$\dot{y}$	$\dot{z}$
Halo $L_1$	0.0E+00	8.79724315850E-03	0.0E+00
Halo $L_2$	0.0E+00	9.7505968672E-03	0.0E+00
	Period		
Halo $L_1$	3.06024482087E+00		
Halo $L_2$	3.10252118223039E+00		

Table 2: Initial conditions and periods for the two Halo orbits around  $L_1$  and  $L_2$  used to perform the transfer between their manifolds. Values are expressed in the normalized system of unit of the {Sun-Earth} system.

Once again, the same method is followed, and perform the computation as easily as in the previous case. The different projections of the intersection with the Poincaré cut  $U_2$  are plotted in Figure 11.

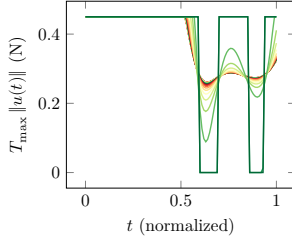
As previously, the two terminal points  $\xi_0^U$  and  $\xi_1^U$  are computed such that they minimize the distance between the two invariant manifolds and the normalized time of propagation (backward and forward) are chosen to build the end-points of the transfer  $\xi_0^*$  and  $\xi_1^*$ . See Figure 12 for the plot of the manifolds and the two natural trajectories (*i.e.* without control). Here, we have chosen  $t_{\mathcal{A}_0} = t_{\mathcal{A}_1} = 0.5$ . This corresponds to approximately 58 days in total. The starting thrust is set to 60 N to reach a targeted thrust of 0.3 N.

The final state continuation is smooth and fast thanks to the rather large initial maximal thrust (see Figure 13a). Then, the thrust continua-



(a) Norm of the control in Newton during the final state continuation. (19 iterations)

(b) Norm of the control in Newton during the thrust continuation. Before reaching a maximal thrust below 0.55 N nothing changes. The last step of the continuation saturates the control. (20 iterations)



(c) Norm of the control in Newton during the continuation from the  $L^2$ -norm of the control to the  $L^1$ -norm. A bang-bang control is finally obtained. (22 iterations)

Figure 10: Different continuations during the resolution of the transfer between invariant manifolds in the {Earth-Moon} system. The different colors are for the steps of the continuations.

tion is easier than for the {Earth-Moon} system, indeed, here the maximal thrust is never reached, and so, this continuation does not change the control at all (see Figure 13b).

The continuation between the  $L^2$ -minimization and the  $L^1$ -minimization is straightforward. Note that a different structure for the bang-bang control is obtained, and here, this continuation does not begin with a saturated control.

Finally, an optimal trajectory is obtained. As before, the initial mass is 1500 kg, and the final mass is 1490.1144 kg. The computational time on a standard desktop computer is 21.86 s for the entire computation of the transfer (from initial states computation to the last continuation on the cost). The final optimal trajectory is plotted in Figure 12 and the different controls for the different continuations are plotted in Figure 13.

### C. Study of the Transfer Time Parameter

One of the parameters the user has to choose is the transfer time. Of course, the larger the transfer time, the lower the cost ( $L^1$ -norm or  $L^2$ -norm). Moreover, it seems intuitive that the larger the time, the lower the maximum of the control norm during the transfer. A numerical study of the influence of this parameter is performed for the two transfers previously introduced: the transfer between invariant manifolds from Halo orbits in the {Sun-Earth} and {Earth-Moon} systems.

The time parameter is varied to test in different cases the efficiency of our algorithm. The states  $\xi_0^U$  and  $\xi_1^U$  defined for the two transfer problems are chosen such that the two states minimize the distance in position and velocity (see Section A). Then a sequence  $(t_f^i)_{i \in \{1, \dots, N\}}$  is chosen discretizing interval  $[0.001, 2.914]$  and the algorithm is executed for each  $t_f^i$ . Using the notation defined in the previous section, we choose for all  $i \in \{1, \dots, N\}$ ,  $t_{M_0}^i = t_{M_1}^i = t_f^i/2$ . The method is efficient and succeeds for almost every  $t_f^i$ . In Figure 14 three sets of tests for the {Sun-Earth} system are plotted and in Figure 15 for the {Earth-Moon}

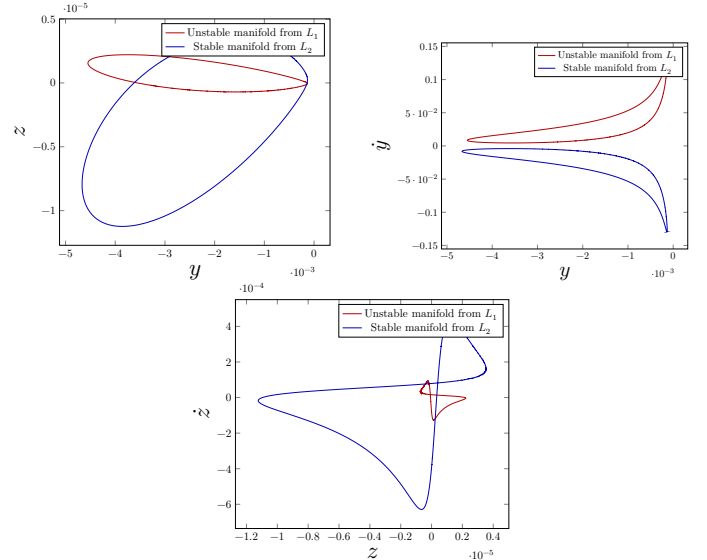


Figure 11: {Sun-Earth} system: Different projections of the intersection with the Poincaré cut  $U_2$  for the invariant manifolds associated with the two Halo orbits around  $L_1$  and  $L_2$ . Note that there is no intersection between the two manifolds, this is obvious on the  $(y, \dot{y})$ -plane projection.

system. First, the control for small times is plotted, when the norm of the control is high and looks like an impulse  $\Delta V$ . The second set is a control for longer times (similar to the control obtained in the previous section). We observe that when the transfer time increases, the method fails for a certain time interval. For the {Earth-Moon} system, the interval is  $I_{EM} = [1.724, 2.224]$  and for the {Sun-Earth} system the interval is  $I_{SE} = [2.126, 2.526]$ .

Note that these two intervals are discrete approximations. When this interval is passed, then the method succeeds again but it gives a different structure of the control and we observe that the optimal trajectories obtained have one revolution around the second primary (respectively Earth and Moon). There is a bifurcation in the structure of the optimal trajectory with respect to the time parameter. The different trajectories for the two systems are plotted in 16a and 16b.

*The time parameter is crucial. It has to be picked it very carefully to obtain the desired result. Note that, whereas there is an interval in which our method fails, it succeeds for a very large range and so, it is not difficult to pick a suitable time using the method described in section VII. It is well known that choosing a transfer duration can be done by solving the minimal time transfer problem. By following the natural dynamics, our method allows to pick an a priori reasonable transfer time.*

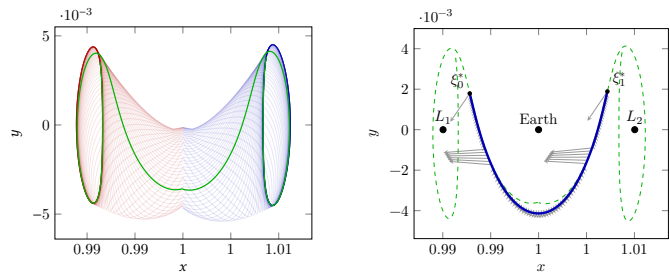
Finally, because one can expect that when the transfer time goes to zero ( $t_f \rightarrow 0$ ), the control converge to the equivalent  $\Delta V$  corresponding to an impulse transfer, in Figure 17, the sequence of  $\eta_i$  is plotted, defined by

$$\eta_i = \left\| \int_0^{t_f^i} \epsilon_* \frac{\|u(t)\|}{m(t)} dt - \Delta V \right\|,$$

where  $\Delta V$  is defined by  $\Delta V = \|\mathbf{v}_0^U - \mathbf{v}_1^U\|$ , with  $\xi_0^U = (\mathbf{x}_0^U, \mathbf{v}_0^U)$  and  $\xi_1^U = (\mathbf{x}_1^U, \mathbf{v}_1^U)$ . In both considered examples, the control converges to the  $\Delta V$  when the transfer time decreases. Note that, because there is also a  $\Delta \mathbf{x}$  for the {Earth-Moon} example, it can be expected that the convergence may not be to  $\Delta V$  exactly. However, the main gap concerns the velocity, hence, in both case the Figure 17 shows that when  $t_f$  goes to 0, then  $\eta_i \rightarrow 0$ . This is coherent with the construction of the problem recalling that an optimal control problem is designed starting with an impulse transfer between the two invariant manifolds.

### Conclusion

To conclude, a general new algorithm has been designed (and a software written in C++) that performs the transfer between two invariant



(a) Intersection of the two invariant manifolds, and the two trajectories that correspond to the two computed points  $\xi_0^U$  and  $\xi_1^U$  that minimize the distance between the two sections.

(b) Optimal solutions for the transfer between the two invariant manifolds. The solutions for the minimization of the  $L^2$ -norm of the control and the solution for the  $L^1$ -norm overlap because of the tiny difference between them.

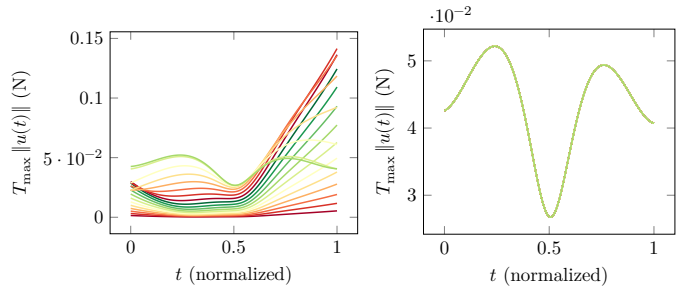
Figure 12: {Sun-Earth} system: Construction and solution of the transfer problem between the two invariant manifolds of two Halo orbits around  $L_1$  and  $L_2$ .

manifolds. This relies on a few parameters that the user has to choose. Of course, because the criterion to be minimized is the norm of the control ( $L^2$  or  $L^1$ ), the transfer time should be fixed. This is a crucial parameter. The study of the influence of this parameter should be done more precisely. Indeed, the longer the transfer time is, the smaller the cost is, but the drawback is that when one chooses too long a transfer time, the first final state continuation can fail. The experiments show that there exist some values of time for which our method fails but these times are sort of transition times between two structures of the trajectory with or without a revolution around the second primary. Outside these time interval, the method is robust and succeeds for a large range of transfer times. Moreover, one can observe that when the transfer time goes to 0, it seems that the control converges to the impulse control as expected. This numerical test checks if the method is robust, and show that the two problems, impulse and low-thrust one, are somehow mathematically connected. Finally, on our two experiments, the behavior with respect to the time parameter is independent of the considered CRTBP.

This algorithm and this method can constitute a brick for designing interplanetary missions using invariant manifolds, and more precisely the Interplanetary Transport Network. Indeed, this allows to reach trajectories of invariant manifolds, and when intersections of invariant manifolds exist, to pass from one to another. A partial application of this algorithm is used in [34] for a complete mission. This could be a good first step to initialize missions patching three body problems with some uncontrolled parts (trajectories in invariant manifolds) and some controlled parts computed by this method to connect the invariant manifolds.

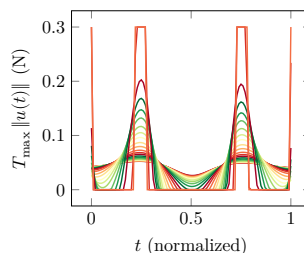
## References

- [1] Koon, W. S., Lo, M. W., Marsden, J. E., and Ross, J. E., *Dynamical Systems, the Three-Body Problem, And Space Mission Design*, Springer-Verlag New York Inc, 2006.
- [2] Caillau, J.-B. and Daoud, B., “Minimum Time Control of the Restricted Three-Body Problem,” *SIAM Journal on Control and Optimization*, Vol. 50, No. 6, 2012, pp. 3178–3202.
- [3] Caillau, J.-B., Daoud, B., and Gergaud, J., “Minimum fuel control of the planar circular restricted three-body problem,” *Celestial Mech. Dynam. Astronom.*, Vol. 114, No. 1-2, 2012, pp. 137–150.
- [4] Zhang, C., Toppoto, F., Bernelli-Zazzera, F., and Zhao, Y.-S., “Low-Thrust Minimum-Fuel Optimization in the Circular Restricted Three-Body Problem,” *Journal of Guidance, Control, and Dynamics*, Vol. 38, No. 8, 2015, pp. 1501–1510, doi: 10.2514/1.G001080.
- [5] Epenoy, R., “Optimal long-duration low-thrust transfers between libration point orbits,” *IAC-2012*, 2012.
- [6] Epenoy, R., *Recent Advances in Celestial and Space Mechanics*, chap. Low-Thrust Transfers Between Libration Point Orbits Without Explicit



(a) Norm of the control in Newton during the final state continuation. (19 iterations)

(b) Norm of the control in Newton during the thrust continuation. Note that the control is never saturated. (19 iterations)



(c) Norm of the control in Newton during the continuation from the  $L^2$ -norm of the control to the  $L^1$ -norm. A bang-bang control is eventually obtained. (25 iterations)

Figure 13: Different continuations during the resolution of the transfer between invariant manifolds in the {Sun-Earth} system. The different colors are for the steps of the continuations.

Use of Manifolds, Springer International Publishing, Cham, 2016, pp. 143–178.

- [7] Gómez, G., Llibre, J., Martínez, R., and Simó, C., *Dynamics and mission design near libration points. Vol. I*, Vol. 2 of *World Scientific Monograph Series in Mathematics*, World Scientific Publishing Co., Inc., River Edge, NJ, 2001, Fundamentals: the case of collinear libration points, With a foreword by Walter Flury.
- [8] Gómez, G., Simó, C., Llibre, J., and Martínez, R., *Dynamics and mission design near libration points. Vol. II*, Vol. 3 of *World Scientific Monograph Series in Mathematics*, World Scientific Publishing Co., Inc., River Edge, NJ, 2001, Fundamentals: the case of triangular libration points.
- [9] Gómez, G., Simó, C., Llibre, J., and Martínez, R., *Dynamics and mission design near libration points. Vol. II*, Vol. 3 of *World Scientific Monograph Series in Mathematics*, World Scientific Publishing Co., Inc., River Edge, NJ, 2001, Fundamentals: the case of triangular libration points.
- [10] Gómez, G., Jorba, A., Simó, C., and Masdemont, J., *Dynamics and mission design near libration points. Vol. IV*, Vol. 5 of *World Scientific Monograph Series in Mathematics*, World Scientific Publishing Co., Inc., River Edge, NJ, 2001, Advanced methods for triangular points.
- [11] Conley, C. C., “Low Energy Transit Orbits in the Restricted Three-Body Problems,” *SIAM Journal on Applied Mathematics*, Vol. 16, No. 4, 1968, pp. 732–746.
- [12] Koon, W. S., Lo, M. W., Marsden, J. E., and Ross, S. D., “Heteroclinic connections between periodic orbits and resonance transitions in celestial mechanics,” *Chaos: An Interdisciplinary Journal of Nonlinear Science*, Vol. 10, No. 2, 2000, pp. 427–469.
- [13] Gomez, G. and Masdemont, J., “Some Zero Cost Transfers between Libration Point Orbits,” *POINT ORBITS, AAS PAPER 00-177, AAS/AIAA ASTRODYNAMICS SPECIALIST CONFERENCE*, 2000.
- [14] Zazzera, F. B., Toppoto, F., and Massari, M., “Assessment of mission design including utilisation of libration points and weak stability boundaries,” Tech. Rep. 03-4103b, European Space Agency, the Advanced Concepts Team, 2004, Available on line at [www.esa.int/act](http://www.esa.int/act).

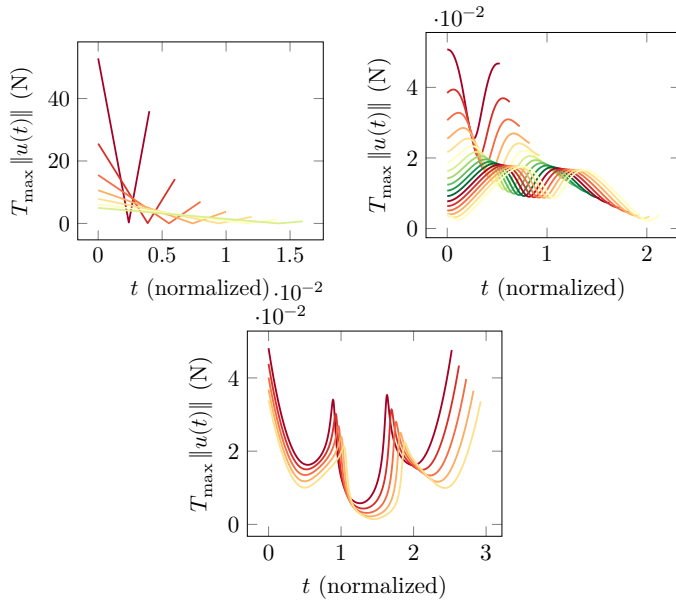


Figure 14: Controls for different transfer times for the transfer between invariant manifolds from Halo orbits in the {Sun-Earth} system. Left: Small times, similar to  $\Delta V$ . Center: Longer times. Right: After the interval  $I_{SE}$ , where the algorithm fails, a different structure for the control is obtained corresponding to a trajectory with a revolution. The different colors are for the steps of the continuations.

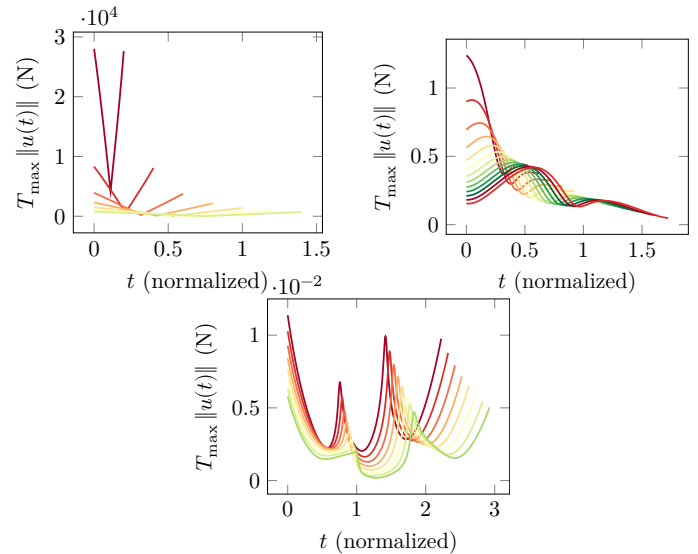


Figure 15: Controls for different transfer times for the transfer between invariant manifolds from Halo orbits in the {Earth-Moon} system. Left: small times, similar to  $\Delta V$ . Center: Longer times. Right: After the interval  $I_{SE}$ , where the algorithm fails, a different structure for the control is obtained corresponding to a trajectory with a revolution. The different colors are for the steps of the continuations.

- [15] Belbruno, E. A. and Miller, J. K., “Sun-perturbed Earth-to-moon transfers with ballistic capture,” *Journal of Guidance Control Dynamics*, Vol. 16, Aug. 1993, pp. 770–775.
- [16] Ross, S. D., “The interplanetary transport network,” *American Scientist*, Vol. 94, No. 3, 2006, pp. 230–237.
- [17] Mingotti, G., Topputo, F., and Bernelli-Zazzera, F., “Low-energy, low-thrust transfers to the Moon,” *Celestial Mechanics and Dynamical Astronomy*, Vol. 105, No. 1-3, 2009, pp. 61–74.
- [18] Mingotti, G., Topputo, F., and Bernelli-Zazzera, F., “Optimal Low-Thrust Invariant Manifold Trajectories via Attainable Sets,” *Journal of guidance, control, and dynamics*, Vol. 34, 2011, pp. 1644–1655.
- [19] Mingotti, G., Topputo, F., and Bernelli-Zazzera, F., “Combined Optimal Low-Thrust and Stable-Manifold Trajectories to the Earth-Moon Halo Orbits,” *AIP Conference Proceedings*, Vol. 886, No. 1, 2007, pp. 100–112.
- [20] Martin, C. and Conway, B. A., “Optimal Low-Thrust Trajectories Using Stable Manifolds,” *Spacecraft Trajectory Optimization*, edited by B. A. Conway, Cambridge University Press, 2010, p. 238–262, Cambridge Books Online.
- [21] Betts, J. T., *Practical Methods for Optimal Control Using Nonlinear Programming*, SIAM, 2001.
- [22] Trélat, E., “Optimal control and applications to aerospace: some results and challenges,” *J. Optim. Theory Appl.*, Vol. 154, No. 3, 2012, pp. 713–758.
- [23] Senent, J., Ocampo, C., and Capella, A., “Low-Thrust Variable-Specific-Impulse Transfers and Guidance to Unstable Periodic Orbits,” *Journal of Guidance, Control, and Dynamics*, Vol. 28, No. 2, 2005, pp. 280–290, doi: 10.2514/1.6398.
- [24] Ozimek, M. T. and Howell, K. C., “Low-Thrust Transfers in the Earth-Moon System, Including Applications to Libration Point Orbits,” *Journal of Guidance, Control, and Dynamics*, Vol. 33, No. 2, 2010, pp. 533–549, doi: 10.2514/1.43179.
- [25] Ocampo, C. and Rosborough, G., *Optimal low-thrust transfers between a class of restricted three-body trajectories*, Vol. 85, Publ by Univelt Inc, pt 2 ed., 1993, pp. 1547–1566.
- [26] Pontryagin, L., Boltianski, V., Gamkrélidzé, R., and Michtchenko, E., *Théorie mathématique des processus optimaux*, 1974.
- [27] Lee, E. B. and Markus, L., *Foundations of optimal control theory*, Robert E. Krieger Publishing Co., Inc., Melbourne, FL, 2nd ed., 1986.

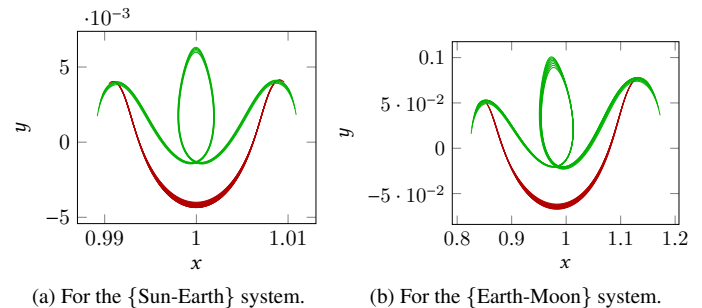
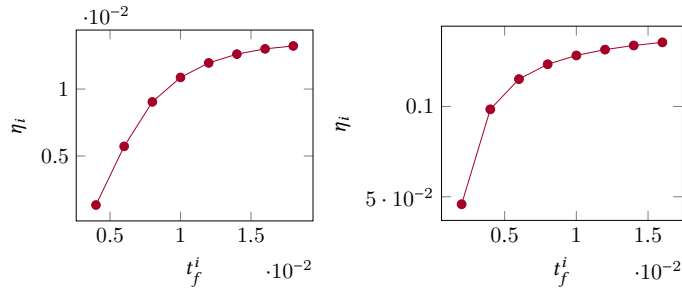


Figure 16: Different optimal trajectories for the two considered systems. A bifurcation can be observed when the time increases, after respectively  $I_{SE}$  and  $I_{EM}$ , the trajectories perform a revolution around the second primary.

- [28] Trélat, E., *Contrôle optimal*, Mathématiques Concrètes. [Concrete Mathematics], Vuibert, Paris, 2005, Théorie & applications. [Theory and applications].
- [29] Haberkorn, T., *Transfert orbital a pousse faible avec minimisation de la consommation: resolution par homotopie differentielle*, Thèse de doctorat, Institut National Polytechnique de Toulouse, Toulouse, France, octobre 2004.
- [30] Jiang, F., Baoyin, H., and Li, J., “Practical Techniques for Low-Thrust Trajectory Optimization with Homotopic Approach,” *Journal of Guidance, Control, and Dynamics*, Vol. 35, No. 1, 2012, pp. 245–258, doi: 10.2514/1.52476.
- [31] Bertrand, R. and Epenoy, R., “New smoothing techniques for solving bang–bang optimal control problems—numerical results and statistical interpretation,” *Optimal Control Applications and Methods*, Vol. 23, No. 4, 2002, pp. 171–197.
- [32] Gergaud, J. and Haberkorn, T., “Homotopy Method for minimum consumption orbit transfer problem,” *ESAIM : Control, Optimisation and Calculus of Variations*, Vol. 12, No. 2, avril 2006, pp. 294–310.
- [33] Cots, O., Caillaud, J.-B., and Gergaud, J., “Differential pathfollowing for regular optimal control problems,” *Optim. Methods Software*, Vol. 27, No. 2, 2012, pp. 177–196.



(a) For the {Sun-Earth} system.

(b) For the {Earth-Moon} system.

Figure 17: Evolution of the sequence  $(\eta_i)_{i \in I}$ . In both cases, we observe that the cost converges to the impulse when the transfer time goes to zero.

- [34] Chupin, M., Haberkorn, T., and Trélat, E., “Low-Thrust Lyapunov to Lyapunov and Halo Missions with  $L^2$ -Minimization,” *ESAIM: Mathematical Modelling and Numerical Analysis*, June 2016, accepted.
- [35] Richardson, D. L., “Analytic Construction of periodic orbits about the collinear points,” Vol. 22, No. 3, oct 1980.
- [36] Archambeau, G., Augros, P., and Trélat, E., “Eight-shaped Lissajous orbits in the Earth-Moon system,” *Mathematics in Action*, Vol. 4, No. 1, 2011, pp. 1–23.
- [37] Jorba, À. and Masdemont, J., “Dynamics in the center manifold of the collinear points of the Restricted Three Body Problem,” 1997.
- [38] Farquhar, R. W. and Kamel, A. A., “Quasi-periodic orbits about the translunar libration point,” *Celestial mechanics*, Vol. 7, No. 4, 1973, pp. 458–473.
- [39] Euler, L., “De motu rectilineo trium corpörum se mutuo attrahentium,” Vol. Oeuvres, Seria Secunda tome XXv Commentationes Astronomicae, 1767, pp. 144–151.
- [40] Lagrange, J.-L., “Essai sur le problème des trois corps,” Vol. Oeuvres de Lagrange 6, Gauthier-Villars, 1772, pp. 272–282.
- [41] Szebehely, V. G., *Theory of Orbits - The Restricted Problem of Three Bodies*, Academic Press, 1967.
- [42] Meyer, K., Hall, G., and Offin, D., *Introduction to Hamiltonian Dynamical Systems and the N-Body Problem*, Applied Mathematical Sciences, Springer New York, 2010.
- [43] Bonnard, B., Faubourg, L., and Trélat, E., *Mécanique céleste et contrôle des véhicules spatiaux*, Vol. 51 of *Mathématiques & Applications (Berlin) [Mathematics & Applications]*, Springer-Verlag, Berlin, 2006.
- [44] Chupin, M., *Interplanetary transfers with low consumption using the properties of the restricted three body problem*, Theses, Université Pierre et Marie Curie - Paris VI, Oct. 2016, tel-01389197.
- [45] Jurdjevic, V., *Geometric Control Theory*, Cambridge Studies in Advanced Mathematics, Cambridge University Press, 1997.
- [46] Bonnard, B., Caillaud, J.-B., and Trélat, E., “Geometric optimal control of elliptic Keplerian orbits,” *Discrete Contin. Dyn. Syst. Ser. B*, Vol. 5, No. 4, 2005, pp. 929–956.
- [47] Caillaud, J.-B. and Noailles, J., “Coplanar control of a satellite around the Earth,” *ESAIM Control Optim. Calc. Var.*, Vol. 6, 2001, pp. 239–258.
- [48] Bonnard, B. and Chyba, M., *Singular Trajectories and Their Role in Control Theory*, Mathématiques et Applications, Springer, 2003.
- [49] Watson, L., *HOMPACK90: FORTRAN 90 Codes for Globally Convergent Homotopy Algorithms*, Department of Computer Science, Virginia Polytechnic Institute and State University, 1996.
- [50] Hairer, E., Nørsett, S., and Wanner, G., *Solving Ordinary Differential Equations I: Nonstiff Problems*, Springer Series in Computational Mathematics, Springer Berlin Heidelberg, 2008.
- [51] Hascoët, L. and Pascual, V., “The Tapenade Automatic Differentiation tool: Principles, Model, and Specification,” *ACM Transactions On Mathematical Software*, Vol. 39, No. 3, 2013.